

Particle Spectroscopy of Supersymmetric $SO(10)$ with Non-Universal Gaugino Masses

Nobuchika Okada ^{a,*}, Shabbar Raza ^{b,†} and Qaisar Shafi ^b

^a *Department of Physics and Astronomy, University of Alabama, Tuscaloosa, AL 35487, USA*

^b *Bartol Research Institute, Department of Physics and Astronomy, University of Delaware, Newark, DE 19716, USA*

We examine the low scale particle spectroscopy of an $SO(10)$ (or equivalently $SU(5)$) inspired supersymmetric model with non-universal gaugino masses. The model assumes minimal supergravity and contains the same number of fundamental parameters as the constrained minimal supersymmetric model (CMSSM.) Realistic solutions compatible with dark matter and other applicable experimental constraints are shown to exist for both positive and negative signs of the MSSM parameter μ . We present several benchmark points which will be tested at the LHC and by the ongoing direct and indirect dark matter detection experiments.

PACS numbers: 12.60.Jv, 12.10.Dm, 14.80.Ly

I. INTRODUCTION

The constrained minimal supersymmetric model (CMSSM), also referred to as mSugra, is based on the standard model gauge symmetry $SU(3) \times SU(2) \times U(1)$ and has the fewest number of fundamental parameters arising from the supersymmetric extension of the SM. Supersymmetry breaking in the CMSSM originates in some unspecified ‘hidden’ sector, which is then transmitted through gravity to our ‘visible’ sector. The lightest neutralino (LSP) in the CMSSM is stable and a leading dark matter candidate particle. Intense searches including direct, indirect and at the LHC, are currently underway to find the LSP. A flurry of recent papers by the ATLAS [1] and CMS [2] experiments at the LHC are beginning to constrain the CMSSM parameter space, which translates into new lower bounds on a variety of sparticle masses including the gluino and the squarks of the first two families.

The apparent unification at $M_G \sim 3 \times 10^{16}$ GeV of the CMSSM gauge couplings strongly suggests the presence of an underlying grand unified theory (GUT) such as $SU(5)$ or $SO(10)$. Since the three MSSM gauge multiplets reside in a single unified gauge multiplet of $SU(5)$ or $SO(10)$, it would seem quite natural that the various MSSM gauginos all acquire the same universal mass $M_{1/2}$ at M_G . However, the universal gaugino mass assumption is, in fact, not a general consequence of gravity mediated SUSY breaking. In the gravity mediation scenario, the gaugino masses are given by non-zero F -term of the gauge kinetic function which, generally, is in one of the irreducible representations of a symmetric product of two adjoint representations and hence, not necessarily a singlet. Therefore, if such a non-singlet develops a non-zero F -term, the MSSM gaugino masses can be expected to be non-universal. Interestingly, if we assume that a single non-zero F -term dominates the gauge kinetic function, the ratios between the MSSM gaugino masses are completely determined by group theory, depending only on the way the MSSM gauge multiplets are embedded in the symmetric product of two adjoint representations of the GUT gauge group. This means that the number of free parameters in a setup with non-universal gaugino masses (NUGM) remains the same as in the CMSSM, at least in the gauge sector.

In the MSSM, the lightest neutralino, if it is the LSP, is a primary candidate for the dark matter particle. Since the neutralino is an admixture of gauginos and Higgsinos, its mass and interaction with other (s)particles are determined by the masses of bino, wino and Higgsinos. Thus, a boundary condition involving non-universal gaugino masses can dramatically alter the phenomenology of neutralino dark matter from the CMSSM case [3]. In addition, the neutralino LSP plays a key role in the SUSY search at high energy colliders, and composition and mass of the neutralino being different from the CMSSM case has impact on SUSY searches at the Tevatron [4] and at the Large Hadron Collider (LHC) [5].

In this paper, we investigate the TeV scale particle spectroscopy of SUSY $SO(10)$ and $SU(5)$ inspired model with non-universal gaugino masses. Taking a variety of phenomenological constraints into account, in particular, the relic density of neutralino dark matter, we identify the allowed regions of the input SSB parameters for various $\tan \beta$ values. We consider both signs of the MSSM μ -parameter. For the allowed parameter region, we calculate the spin-independent (SI) and spin-dependent (SD) cross sections for neutralino elastic scattering off a nucleon, and compare our results with the current and proposed future bounds from direct and indirect dark matter search experiments. We also present several benchmark points from the allowed region and show the sparticle mass spectra, which can be tested at the LHC. The mass spectra are compared with those from the CMSSM with suitably fixed parameter sets.

*Electronic address: okadan@ua.edu.

†Electronic address: shabbar@udel.edu. On study leave from: Department of Physics, FUUAST, Islamabad, Pakistan.

II. NON-UNIVERSAL GAUGINO MASSES FROM $SO(10)$ AND $SU(5)$

We first review how the non-universal gaugino masses arise in the $SO(10)$ GUT. In gravity mediation, we introduce a higher dimensional operator between the gauge field strength superfield \mathcal{W}^a and a hidden sector chiral superfield Φ_{ab} ,

$$\mathcal{L} = \int d^2\theta \frac{\Phi_{ab}}{M_P} \mathcal{W}^a \mathcal{W}^b, \quad (1)$$

where $a, b = 1, 2, \dots, 45$ are the group indices for $SO(10)$, and $M_P = 2.4 \times 10^{18}$ GeV is the reduced Planck mass. In this paper, we consider only a single hidden sector field Φ_{ab} whose non-zero F -term breaks SUSY and generates the gaugino masses:

$$\mathcal{L} = \int d^2\theta \frac{\Phi_{ab}}{M_P} \mathcal{W}^a \mathcal{W}^b \supset \frac{F_{\Phi_{ab}}}{M_P} \lambda^a \lambda^b. \quad (2)$$

In $SO(10)$, a possible representation of the hidden sector field is given by one of the irreducible representations contained in the symmetric product of two adjoint 45-dimensional representations:

$$(45 \otimes 45)_{\text{sym}} = \mathbf{1} \oplus \mathbf{54} \oplus \mathbf{210} \oplus \mathbf{770}. \quad (3)$$

If the hidden sector field is not the singlet, non-universal masses for the MSSM gauginos are generated. However, the ratio between the MSSM gaugino masses is determined by the embedding of the SM gauge groups within each irreducible representation [6, 7].

Among the three possibilities in Eq.(3), we investigate Φ_{ab} in the $\mathbf{54}$ representation in this paper. In fact, this is the most reasonable case from the theoretical point of view. We are considering SUSY $SO(10)$ as a more fundamental theory within which the MSSM is embedded. We may expect that the $SO(10)$ model is further unified into a more fundamental theory including gravity, most likely some string theory at the Planck scale. Note that this picture constrains the field representations introduced in the model, since large representations carry a large β -function, and this can cause the $SO(10)$ gauge coupling to blow up below the Planck scale. Indeed, the introduction of an irreducible representation larger than 126 is excluded by this argument [8]. With the $\mathbf{54}$ -plet of hidden sector field, the ratios of the non-universal gaugino masses is found to be [7]

$$M_1 : M_2 : M_3 = -\frac{1}{2} : -\frac{3}{2} : 1 \quad (4)$$

The above discussion is readily extended to $SU(5)$, and the gluino mass ratios turn out to be the same as in Eq.(4) for a hidden sector field in the 24-dimensional adjoint representation [7]. Thus, our analysis in this paper applies both to $SO(10)$ and $SU(5)$ models. However, note that in the $SU(5)$ GUT, the matter multiplets of each family are not completely unified in a single representation and in general, the masses of sfermions in $\mathbf{5}^*$ and $\mathbf{10}$ representations can be non-universal. This non-universality of sfermion masses can serve as a probe to discriminate the underlying GUT gauge groups [9].

In the following, we identify the parameter region which is consistent with a variety of phenomenological constraints. Since the ratio between the non-universal gaugino masses is fixed as in Eq. (4), the number of free parameters remains the same as in the CMSSM. We use the notation $M_3 = M_{1/2}$, so that $M_1 = -\frac{1}{2}M_{1/2}$ and $M_2 = -\frac{3}{2}M_{1/2}$. The fundamental parameters of the $SO(10)/SU(5)$ model that we consider are as follows:

$$m_0, M_{1/2}, A_0, \tan \beta, \text{sign}(\mu). \quad (5)$$

III. PHENOMENOLOGICAL CONSTRAINTS AND SCANNING PROCEDURE

We employ the ISAJET 7.80 package [10] to perform random scans over the parameter space listed in Eq. (5). In this package, the weak scale values of gauge and third generation Yukawa couplings are evolved to M_{GUT} via the MSSM renormalization group equations (RGEs) in the \overline{DR} regularization scheme. We do not strictly enforce the unification condition $g_3 = g_1 = g_2$ at M_{GUT} , since a few percent deviation from unification can be assigned to unknown GUT-scale threshold corrections [11]. At M_{GUT} , the boundary conditions given in Eq. (5) are imposed and all the SSB parameters, along with the gauge and Yukawa couplings, are evolved back to the weak scale M_Z . The impact of the neutrino Dirac Yukawa coupling in the running of the RGEs is significant only for relatively large values (~ 2 or so) [12]. In the $SO(10)$ GUT we expect the largest Dirac coupling to be comparable to the top Yukawa coupling (~ 0.5 at M_{GUT}) and thus we safely neglect effects of the neutrino Dirac Yukawa coupling in our analysis.

In the evaluation of Yukawa couplings the SUSY threshold corrections [13] are taken into account at the common scale $M_{\text{SUSY}} = \sqrt{m_{\tilde{t}_L} m_{\tilde{t}_R}}$. The entire parameter set is iteratively run between M_Z and M_{GUT} using the full 2-loop RGEs until a

stable solution is obtained. To better account for leading-log corrections, one-loop step-beta functions are adopted for gauge and Yukawa couplings, and the SSB parameters m_i are extracted from RGEs at multiple scales $m_i = m_i(m_i)$. The RGE-improved 1-loop effective potential is minimized at an optimized scale M_{SUSY} , which effectively accounts for the leading 2-loop corrections. Full 1-loop radiative corrections are incorporated for all sparticle masses.

The requirement of radiative electroweak symmetry breaking (REWSB) [14] puts an important theoretical constraint on the parameter space. Another important constraint comes from limits on the cosmological abundance of stable charged particles [15]. This excludes regions in the parameter space where charged SUSY particles, such as $\tilde{\tau}_1$ or \tilde{t}_1 , become the LSP. We accept only those solutions for which one of the neutralinos is the LSP and saturates the dark matter relic abundance bound observed by the Wilkinson Microwave Anisotropy Probe (WMAP).

We perform random scans for the following parameter range:

$$\begin{aligned} 0 &\leq m_0 \leq 5 \text{ TeV} \\ 0 &\leq M_{1/2} \leq 2 \text{ TeV} \\ \tan \beta &= 10, 30, 50 \\ A_0 &= 0, 1, -1, 5, -5 \text{ TeV} \\ \mu &< 0, \mu > 0 \end{aligned} \tag{6}$$

with $m_t = 173.1 \text{ GeV}$ [16]. The results are not too sensitive to one or two sigma variation in the value of m_t . We use $m_b(m_Z) = 2.83 \text{ GeV}$ which is hard-coded into ISAJET.

In scanning the parameter space, we employ the Metropolis-Hastings algorithm as described in [17]. All of the collected data points satisfy the requirement of REWSB, with the neutralino in each case being the LSP. Furthermore, all of these points satisfy the constraint $\Omega_{\text{CDM}} h^2 \leq 10$. This is done so as to collect more points with a WMAP compatible value of cold dark matter (CDM) relic abundance. For the Metropolis-Hastings algorithm, we only use the value of $\Omega_{\text{CDM}} h^2$ to bias our search. Our purpose in using the Metropolis-Hastings algorithm is to be able to search around regions of acceptable $\Omega_{\text{CDM}} h^2$ more fully. After collecting the data, we impose the mass bounds on all the particles [15] and use the IsaTools package [18] to implement the following phenomenological constraints:

$$\begin{aligned} m_h \text{ (lightest Higgs mass)} &\geq 114.4 \text{ GeV} & [19] \\ BR(B_s \rightarrow \mu^+ \mu^-) &< 5.8 \times 10^{-8} & [20] \\ 2.85 \times 10^{-4} \leq BR(b \rightarrow s \gamma) &\leq 4.24 \times 10^{-4} \text{ (} 2\sigma \text{)} & [21] \\ 0.53 \leq \frac{BR(B_u \rightarrow \tau \nu_\tau)_{\text{MSSM}}}{BR(B_u \rightarrow \tau \nu_\tau)_{\text{SM}}} &\leq 2.03 \text{ (} 2\sigma \text{)} & [22] \\ \Omega_{\text{CDM}} h^2 &= 0.111_{-0.037}^{+0.028} \text{ (} 5\sigma \text{)} & [23] \\ 3.4 \times 10^{-10} \leq \Delta(g-2)_\mu/2 &\leq 55.6 \times 10^{-10} \text{ (} 3\sigma \text{)} & [24] \end{aligned}$$

We apply the experimental constraints successively on the data that we acquire from ISAJET.

IV. RESULTS

Figure 1 shows the results in the $(M_{1/2}, m_0)$ plane for $\tan \beta = 10$, $A_0 = 0$ and $\text{sign}(\mu) = \pm$. Gray points are consistent with successful REWSB and the requirement of neutralino LSP. Blue points satisfy the WMAP bounds on neutralino dark matter abundance, particle mass bounds, as well as constraints from $BR(B_s \rightarrow \mu^+ \mu^-)$, $BR(b \rightarrow s \gamma)$ and $BR(B_u \rightarrow \tau \nu_\tau)$. In Figure 1, the small boxes show benchmark points for each of which the particle mass spectra are listed in Tables I and II. We have chosen these benchmark points from regions in Figure 2 and 3, which can be explored by future dark matter search experiments (see below).

A variety of experiments are underway to directly detect dark matter particles through their elastic scatterings off nuclei. The most stringent limits on the (spin-independent) elastic scattering cross section have been reported by the recent CDMS-II and XENON100 experiments. In Figure 2 (the color coding is the same as in Figure 1) we show the results for the spin-independent elastic scattering cross section along with the current upper bounds by the CDMS-II [25] (solid black line) and XENON100 [26] (solid red line) experiments, as well as the future reach of the SuperCDMS(SNOLAB) [27] (dotted black line) and XENON1T [28] (dotted red line). In the $(\sigma_{\text{SI}}, m_{\tilde{\chi}_1^0})$ plane, there are dips in the resultant cross sections. Two of them around $m_{\tilde{\chi}_1^0} \sim 45 \text{ GeV}$ and $m_{\tilde{\chi}_1^0} \sim 57 \text{ GeV}$ correspond to Z- and Higgs resonances, respectively. Around these parameter regions, the neutralino annihilation cross sections are enhanced by the resonances and as a result, the correct relic abundance can be achieved with relatively small coupling constants. Thus, the corresponding spin-independent cross sections are reduced due to the small coupling constants. Another dip around $m_{\tilde{\chi}_1^0} \sim 200 \text{ GeV}$ in Figure 2 (a) corresponds to a cancellation between effective couplings of neutralino with up-quark and down-quark in Higgs exchange processes. As has been reported in [29], this cancellation occurs when the relative signs between $M_{1,2}$ and μ are opposite. Recall that in our convention, $M_3 > 0$ and

$M_{1/2} < 0$, so that this cancellation occurs for $\mu > 0$. The small boxes show the benchmark points corresponding to those listed in Tables I and II. These benchmark points have been chosen with the criterion that they should lie between the present experimental limits and future reaches. In the region from which the benchmark points are chosen, the neutralino LSP has sizable Higgsino components which, in turn, enhance the spin-independent neutralino-nucleon cross sections. All of the benchmark points can be tested by XENON1T, while SuperCDMS can explore some of them.

Neutralino dark matters in the galactic halo may become gravitationally trapped in the Sun and accumulate in its center, where they can annihilate each other and produce high energy neutrinos. Since neutrinos can escape and reach the Earth, the neutralino annihilations can be indirectly detected by observing an excess of such high energy neutrinos from the Sun. The most stringent limits on the neutrino flux from the Sun have been reported by Super-Kamiokande [30] and IceCube [31] experiments, which provide the upper limit on the spin-dependent elastic scattering cross section of neutralino dark matter off a nucleon. The spin-dependent scattering cross sections along with the current upper bounds and future reach are depicted in Figure 3. In this figure too, the color coding is the same as in Figure 1. In the $(\sigma_{SD}, m_{\tilde{\chi}_1^0})$ plane we show the results for the spin-dependent elastic scattering cross section along with the current bounds from Super-Kamiokande (black line) and IceCube (dotted black line) experiments, together with the future reach of IceCube DeepCore experiment (dotted red line). The small boxes show the approximate locations of benchmark points corresponding to Tables I and II. For these points, the sizable Higgsino components of the neutralino LSP enhances the scattering cross section. All benchmark points except for point 1 are testable by the future IceCube DeepCore experiment. Although the benchmark point 1 has a neutralino mass below the energy threshold of the IceCube DeepCore experiment, such a light neutralino can provide characteristic signatures in collider experiments.

Plots analogous to Figures 1-3 for varying values of $\tan \beta$ are shown in Figures 4-9 and the particle mass spectra of the corresponding benchmark points are listed in Tables III-VI. The figures for $\mu < 0$ show green points which belong to the subset of blue points and satisfy all constraints including $\Delta(g-2)_\mu/2$, where the deviation of the muon anomalous magnetic dipole moment from the SM prediction can be explained by sparticle loop contributions. Since the sparticle contributions to $\Delta(g-2)_\mu/2$ are dominated by loop diagrams with chargino and are proportional to $\mu M_2 \tan \beta / \tilde{m}_{SUSY}^4$, where \tilde{m}_{SUSY} is the sparticle mass in the loop, the relative sign of μ and M_2 should be positive ($\mu < 0$ in our convention) in order to obtain $\Delta(g-2)_\mu/2 > 0$. If the sparticles running in the loop diagrams are heavy, a relatively large $\tan \beta$ is necessary to satisfy the constraint from $\Delta(g-2)_\mu/2$. There is no green point in Figure 1 because $\tan \beta = 10$ is too small to be compatible with the $\Delta(g-2)_\mu/2$ constraint. We also list benchmark points (5 and 6 in Tables III-VI) with relatively large neutralino mass, some of which can/cannot be tested by the future IceCube DeepCore experiment.

For $|A_0| \leq \mathcal{O}(1 \text{ TeV})$, the results remain almost the same as those with $A_0 = 0$, and we therefore do not show all plots. The results for special cases with a large A_0 or a large $\tan \beta$ are depicted in Figure 10. The upper panel shows the results in the $(M_{1/2}, m_0)$ plane for $A_0 = -5 \text{ TeV}$, $\tan \beta = 10$ and $\mu < 0$. An almost identical plot is also obtained for the opposite sign of $\mu > 0$. There are two interesting regions. One is the usual stau co-annihilation region for $M_{1/2} \gtrsim 1 \text{ TeV}$, the other one is the region for $M_{1/2} \lesssim 1 \text{ TeV}$ where the mass difference between the neutralino LSP and lighter stop is small, and the desired relic abundance of neutralino dark matter is achieved through stop-neutralino co-annihilations. This stop-neutralino co-annihilation region only appears for a big negative A_0 . The lower panel corresponds to the results for a relatively large $\tan \beta (= 53)$ in the $(m_H, m_{\tilde{\chi}_1^0})$ plane. The allowed region appears for $2m_{\tilde{\chi}_1^0} \simeq m_H$ by the enhancement of neutralino annihilation cross sections via heavy Higgs boson exchange processes in the s -channel. For the chosen benchmark points, the mass spectra are listed in Table VII.

Finally, we choose several benchmark points from the allowed regions for different values of A_0 , $\tan \beta$ and $\text{sign}(\mu)$ and compare the mass spectra in our NUGM model with those from the CMSSM. In Table VIII, we present four benchmark points from the stau-neutralino co-annihilation region to compare the mass spectra. For the same values of A_0 , $\tan \beta$ and $\text{sign}(\mu)$, we tune m_0 and $M_{1/2}$ in the CMSSM in order to obtain the same masses for neutralino LSP and the lighter stau as those found in NUGM model. The resultant masses for the other particles are all larger than those in the CMSSM. In Table IX, we tune m_0 and $M_{1/2}$ in the CMSSM so as to give the same masses for gluino and right-handed down squarks as in the NUGM model. We can see, in this case, large mass differences in the neutralino and chargino mass spectra, while the sfermion mass spectra are similar. In particular, the mass of the neutralino LSP is relatively small as a result of the non-universal boundary conditions for the gaugino masses. The results in these Tables show that the mass spectra in our NUGM model are quite distinct from those in the CMSSM.

V. CONCLUSIONS

We have investigated the low scale particle spectroscopy arising from supersymmetric SO(10) and SU(5) models with non-universal gaugino masses. This non-universality generally arises from the F -term of some non-singlet hidden sector field in the gauge kinetic function in the gravity mediated supersymmetry breaking. Depending on the embedding of the MSSM gauge group, the ratio of the MSSM gaugino masses is determined by group theory. Among several possibilities, we have considered an F -term from a single 54-plet hidden sector field. This is a unique possibility if we require the SO(10) gauge coupling to stay within the perturbative regime up to the Planck scale. With the group theoretically fixed ratios of the gaugino masses, we

set the fundamental parameters of the model in the same way as the CMSSM, namely, m_0 , $M_{1/2}$, A_0 , $\tan\beta$ and $\text{sign}(\mu)$ with the identification $M_3 = M_{1/2}$. Taking a variety of phenomenological constraints into account, we have identified the allowed parameter regions. We have also calculated the spin-independent and dependent cross sections of neutralino elastic scattering off a nucleon and compared the results with the reach of future direct and indirect detection experiments. We have identified the benchmark points of the model which are consistent with the phenomenological constraints and which predict neutralino elastic scattering cross sections accessible at the future dark matter detection experiments. The particle mass spectra of the benchmark points can be well-distinguished at the LHC from the mass spectra in the CMSSM.

Note Added: t - b - τ Yukawa unification in this class of models with $\mu < 0$ has recently been investigated in [32].

Acknowledgments

We thank Ilia Gogoladze and Rizwan Khalid for useful comments and discussion. This work is supported in part by the DOE Grants, No. DE-FG02-10ER41714 (N.O.) and No. DE-FG02-91ER40626 (Q.S. and S.R.) and by Bartol Research Institute (S.R.). N.O. would like to thank the Particle Theory Group of the University of Delaware for hospitality during his visit.

-
- [1] G. Aad *et al.* [Atlas Collaboration], arXiv:1102.2357 [hep-ex]; J. B. G. da Costa *et al.* [Atlas Collaboration], arXiv:1102.5290 [hep-ex].
 - [2] V. Khachatryan *et al.* [CMS Collaboration], Phys. Lett. B **698**, 196 (2011) [arXiv:1101.1628 [hep-ex]].
 - [3] A. Corsetti and P. Nath, Phys. Rev. D **64**, 125010 (2001); S. F. King, J. P. Roberts and D. P. Roy, JHEP **0710**, 106 (2007); K. Huitu and J. Laamanen, Phys. Rev. D **79**, 085009 (2009); U. Chattopadhyay, D. Das and D. P. Roy, Phys. Rev. D **79**, 095013 (2009); M. Holmes and B. D. Nelson, Phys. Rev. D **81**, 055002 (2010).
 - [4] G. Anderson, H. Baer, C. h. Chen and X. Tata, Phys. Rev. D **61**, 095005 (2000).
 - [5] S. Bhattacharya, A. Datta and B. Mukhopadhyaya, JHEP **0710**, 080 (2007); K. Huitu, J. Laamanen, P. N. Pandita and S. Roy, Phys. Rev. D **72**, 055013 (2005); K. Huitu, R. Kinnunen, J. Laamanen, S. Lehti, S. Roy and T. Salminen, Eur. Phys. J. C **58**, 591 (2008); S. Bhattacharya and J. Chakraborty, Phys. Rev. D **81**, 015007 (2010).
 - [6] N. Chamoun, C. S. Huang, C. Liu and X. H. Wu, Nucl. Phys. B **624** (2002) 81 [arXiv:hep-ph/0110332].
 - [7] S. P. Martin, Phys. Rev. D **79**, 095019 (2009) [arXiv:0903.3568 [hep-ph]].
 - [8] D. Chang, T. Fukuyama, Y. Y. Keum, T. Kikuchi and N. Okada, Phys. Rev. D **71**, 095002 (2005).
 - [9] I. Gogoladze, R. Khalid, N. Okada and Q. Shafi, Phys. Rev. D **79**, 095022 (2009); N. Okada and H. M. Tran, Phys. Rev. D **83**, 053001 (2011).
 - [10] H. Baer, F. E. Paige, S. D. Protopopescu and X. Tata, arXiv:hep-ph/0001086.
 - [11] J. Hisano, H. Murayama, and T. Yanagida, Nucl. Phys. **B402** (1993) 46. Y. Yamada, Z. Phys. **C60** (1993) 83; J. L. Chkareuli and I. G. Gogoladze, Phys. Rev. D **58**, 055011 (1998).
 - [12] For recent discussions and additional references see V. Barger, D. Marfatia and A. Mustafayev, Phys. Lett. B **665**, 242 (2008); M. E. Gomez, S. Lola, P. Naranjo and J. Rodriguez-Quintero, arXiv:0901.4013 [hep-ph].
 - [13] D. M. Pierce, J. A. Bagger, K. T. Matchev, and R.-j. Zhang, Nucl. Phys. **B491** (1997) 3.
 - [14] L. E. Ibanez and G. G. Ross, Phys. Lett. **B110** (1982) 215; K. Inoue, A. Kakuto, H. Komatsu and S. Takeshita, Prog. Theor. Phys. **68**, 927 (1982) [Erratum-ibid. **70**, 330 (1983)]; L. E. Ibanez, Phys. Lett. **B118** (1982) 73; J. R. Ellis, D. V. Nanopoulos, and K. Tamvakis, Phys. Lett. **B121** (1983) 123; L. Alvarez-Gaume, J. Polchinski, and M. B. Wise, Nucl. Phys. **B221** (1983) 495.
 - [15] K. Nakamura *et al.* [Particle Data Group], J. Phys. G **37**, 075021 (2010).
 - [16] [Tevatron Electroweak Working Group and CDF Collaboration and D0 Collab], arXiv:0903.2503 [hep-ex].
 - [17] G. Belanger, F. Boudjema, A. Pukhov and R. K. Singh, JHEP **0911**, 026 (2009); H. Baer, S. Kraml, S. Sekmen and H. Summy, JHEP **0803**, 056 (2008).
 - [18] H. Baer, C. Balazs, and A. Belyaev, JHEP **03** (2002) 042; H. Baer, C. Balazs, J. Ferrandis, and X. Tata Phys. Rev. **D64** (2001) 035004.
 - [19] S. Schael *et al.* Eur. Phys. J. C **47**, 547 (2006).
 - [20] T. Aaltonen *et al.* [CDF Collaboration], Phys. Rev. Lett. **100**, 101802 (2008).
 - [21] E. Barberio *et al.* [Heavy Flavor Averaging Group (HFAG) Collaboration], arXiv:0704.3575 [hep-ex].
 - [22] D. Eriksson, F. Mahmoudi and O. Stal, JHEP **0811** (2008) 035.
 - [23] E. Komatsu *et al.* [WMAP Collaboration], Astrophys. J. Suppl. **180**, 330 (2009).
 - [24] G. W. Bennett *et al.* [Muon G-2 Collaboration], Phys. Rev. D **73**, 072003 (2006).
 - [25] Z. Ahmed *et al.* [The CDMS-II Collaboration], arXiv:0912.3592 [astro-ph.CO].
 - [26] E. Aprile *et al.* [XENON100 Collaboration], arXiv:1104.2549 [astro-ph.CO].
 - [27] T. Bruch and f. t. C. Collaboration, arXiv:1001.3037 [astro-ph.IM].
 - [28] The XENON Dark Matter Project http://xenon.astro.columbia.edu/XENON100_Experiment/

- [29] J. R. Ellis, A. Ferstl, K. A. Olive, Phys. Lett. **B481**, 304-314 (2000). [hep-ph/0001005].
- [30] S. Desai *et al.* [Super-Kamiokande Collaboration], Phys. Rev. D **70**, 083523 (2004) [Erratum-ibid. D **70**, 109901 (2004)].
- [31] R. Abbasi *et al.* [ICECUBE Collaboration], Phys. Rev. Lett. **102**, 201302 (2009).
- [32] I. Gogoladze, Q. Shafi and C. S. Un, to appear.

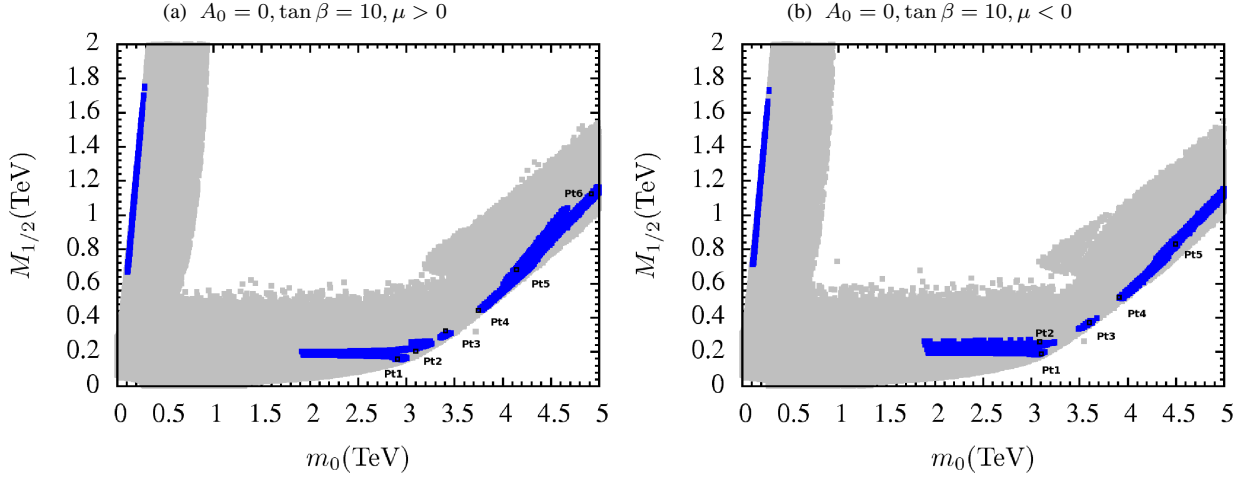


FIG. 1: Plots in the $(M_{1/2}, m_0)$ plane. Gray points are consistent with REWSB and $\tilde{\chi}_1^0$ LSP. Blue points satisfy the WMAP bounds on $\tilde{\chi}_1^0$ dark matter abundance, particle mass bounds, constraints from $BR(B_s \rightarrow \mu^+ \mu^-)$ and $BR(b \rightarrow s\gamma)$ and $BR(B_u \rightarrow \tau \nu_\tau)$. Approximate locations of benchmark points listed in Tables I and II are also shown.

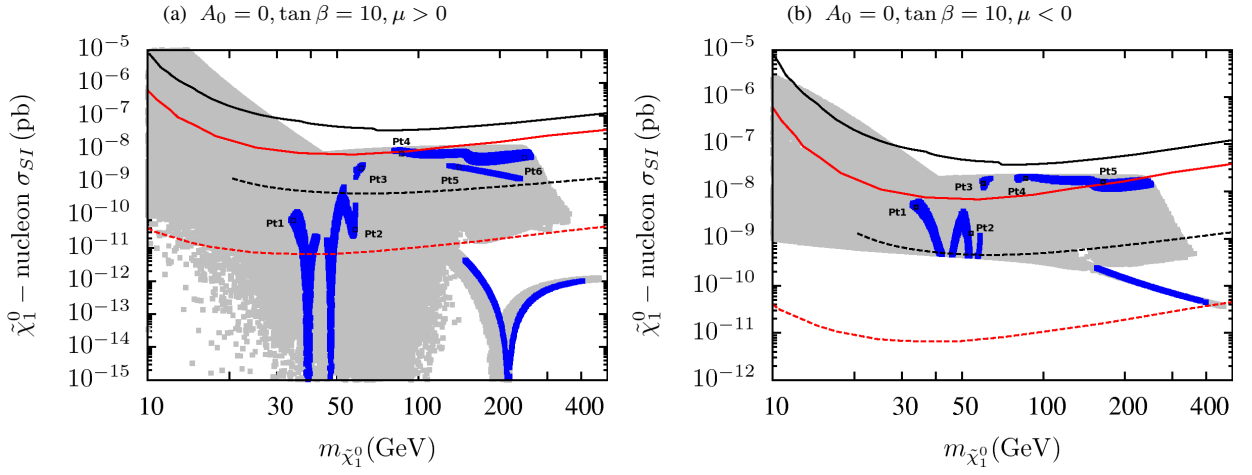


FIG. 2: Spin-independent elastic scattering cross section of neutralino dark matter in the $(\sigma_{SI}, m_{\tilde{\chi}_1^0})$ plane. Color coding is the same as in Figure 1. The current upper bounds from CDMS-II (XENON100) are depicted as black (red) solid lines. Future reach of the SuperCDMS(SNOLAB) (dotted black line) and XENON1T (dotted red line) are shown. Approximate locations of benchmark points listed in Tables I and II are also shown, and which are testable in the ongoing experiments.

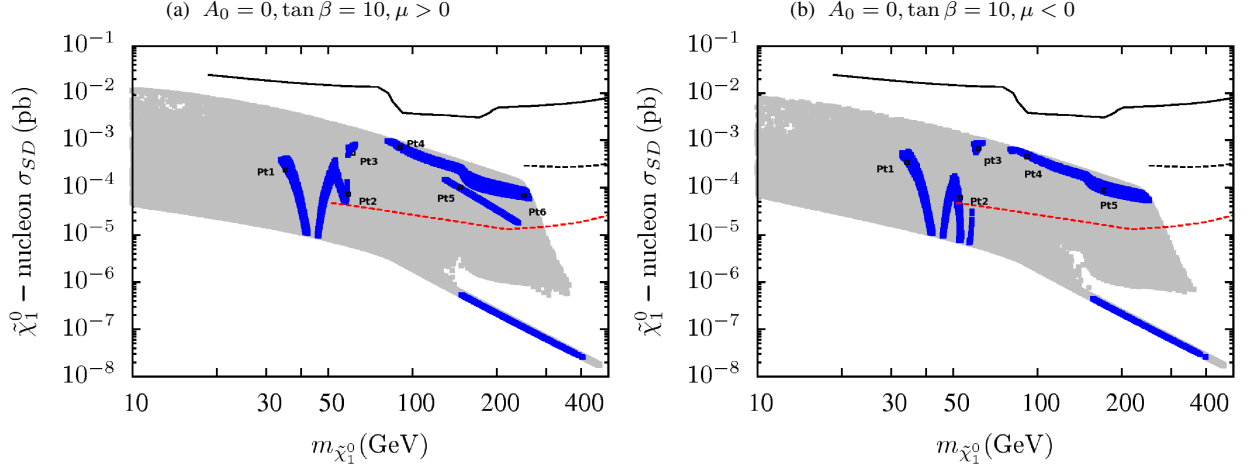


FIG. 3: Spin-dependent elastic scattering cross section of neutralino dark matter in the $(\sigma_{SD}, m_{\tilde{\chi}_1^0})$ plane. Color coding is the same as in Figure 1. Current bounds from Super-Kamiokande (black line), IceCube (dotted black line), and future reach of IceCube DeepCore experiment (dotted red line) are shown. Approximate locations of benchmark points presented in Tables I and II are also shown.

	Pt1	Pt2	Pt3	Pt4	Pt5	Pt6
m_0	2948	3134	3404	3780	4384	4982
$M_{1/2}$	154	250	292	447	778	1166
A_0	0	0	0	0	0	0
$sign(\mu)$	+	+	+	+	+	+
$\tan \beta$	10	10	10	10	10	10
m_h	116	117	118	118	119	119
m_H	2926	3120	3387	3773	4418	5078
m_A	2907	3099	3365	3749	4389	5045
m_{H^\pm}	2927	3121	3388	3774	4419	5079
$m_{\tilde{\chi}_{1,2}^0}$	34,108	56, 176	59,119	81, 121	170, 234	262, 323
$m_{\tilde{\chi}_{3,4}^0}$	138,239	197, 355	127,404	132, 603	238, 1032	330,1537
$m_{\tilde{\chi}_{1,2}^\pm}$	104,233	168, 345	106,391	104, 585	213, 1006	297, 1502
$m_{\tilde{g}}$	490	733	838	1207	1951	2784
$m_{\tilde{u}_{L,R}}$	2936,2946	3150, 3154	3429,3432	3863,3855	4637, 4596	5486,5395
$m_{\tilde{t}_{1,2}}$	1687,2402	1824, 2587	1994,2820	2280,3196	2819, 3884	3433,4657
$m_{\tilde{d}_{L,R}}$	2938,2948	3151, 3156	3430,3434	3864,3857	4638, 4598	5487,5397
$m_{\tilde{b}_{1,2}}$	2395,2921	2577, 3127	2809,3403	3184,3822	3871, 4556	4641,5348
$m_{\tilde{\nu}_1}$	2946	3137	3410	3798	4441	5099
$m_{\tilde{\nu}_3}$	2933	3124	3395	3782	4423	5078
$m_{\tilde{e}_{L,R}}$	2946,2945	3137, 3131	3409,3401	3798,3777	4440, 4382	5097,4982
$m_{\tilde{\tau}_{1,2}}$	2919,2933	3104, 3123	3372,3394	3745,3781	4345, 4421	4940,5076
$\sigma_{SI}(\text{pb})$	6.8×10^{-11}	6.2×10^{-11}	2.4×10^{-9}	8.9×10^{-9}	4.8×10^{-9}	5.7×10^{-9}
$\sigma_{SD}(\text{pb})$	3.8×10^{-4}	8.2×10^{-5}	7.1×10^{-4}	9.9×10^{-4}	1.2×10^{-4}	6.0×10^{-5}
$\Omega_{CDM} h^2$	0.13	0.1	0.10	0.12	0.1	0.13

TABLE I: Mass spectra for the benchmark points with $\tan \beta=10$, $\mu > 0$. All of these points satisfy the various constraints mentioned in section III, except $\Delta(g-2)_\mu/2$. Neutralino LSP in all cases has sizeable higgsino component. The points lie between current and future direct and indirect dark matter search limits shown in Figures 2 and 3. Pt1 represents the lightest neutralino and a light gluino. Pts.2 and 3 also have relatively light gluinos.

	Pt1	Pt2	Pt3	Pt4	Pt5
m_0	3071	3061	3573	3984	4490
$M_{1/2}$	184	249	358	536	855
A_0	0	0	0	0	0
$sign(\mu)$	-	-	-	-	-
$\tan\beta$	10	10	10	10	10
m_h	117	117	118	118	119
m_H	3050	3048	3560	3986	4535
m_A	3030	3028	3536	3960	4505
m_{H^\pm}	3051	3049	3560	3986	4536
$m_{\tilde{\chi}_{1,2}^0}$	33,110	52, 184	62, 122	98, 147	182, 252
$m_{\tilde{\chi}_{3,4}^0}$	134, 278	209, 362	128, 490	163, 720	262, 1133
$m_{\tilde{\chi}_{1,2}^\pm}$	106, 271	185, 355	112, 478	143, 705	255, 1113
$m_{\tilde{g}}$	567	730	998	1424	2119
$m_{\tilde{u}_{L,R}}$	3066, 3074	3078, 3082	3621, 3620	4107, 4091	4791, 4740
$m_{\tilde{t}_{1,2}}$	1765, 2512	1783, 2528	2119, 2985	2443, 3408	2932, 4028
$m_{\tilde{d}_{L,R}}$	3067, 3076	3080, 3084	3620, 3622	4108, 4093	4792, 4742
$m_{\tilde{b}_{1,2}}$	2502, 3048	2518, 3056	2974, 3588	3396, 4056	4011, 4698
$m_{\tilde{\nu}_1}$	3070	3065	3584	4011	4558
$m_{\tilde{\nu}_3}$	3057	3052	3568	3994	4540
$m_{\tilde{e}_{L,R}}$	3070, 3068	3065, 3058	3583, 3570	4011, 3981	4557, 4488
$m_{\tilde{\tau}_{1,2}}$	3041, 3056	3017, 3051	3539, 3567	3947, 3993	4450, 4538
$\sigma_{SI}(\text{pb})$	5.1×10^{-9}	1.7×10^{-9}	1.5×10^{-8}	1.9×10^{-8}	1.2×10^{-8}
$\sigma_{SD}(\text{pb})$	4.8×10^{-4}	6.5×10^{-5}	7.1×10^{-4}	4.1×10^{-4}	7.9×10^{-5}
$\Omega_{CDM}h^2$	0.13	0.11	0.13	0.11	0.12

TABLE II: Mass spectra for the benchmark points for $\tan\beta=10$, $\mu < 0$. All of these points satisfy the various constraints mentioned in section III, except $\Delta(g-2)_\mu/2$. Neutralino LSP in all cases has sizeable higgsino component. The points lie between present and future direct and indirect dark matter search limits shown in Figures 2 and 3. Pt1 represents lightest neutralino, while Pts.1,2,3 have relatively light gluinos.

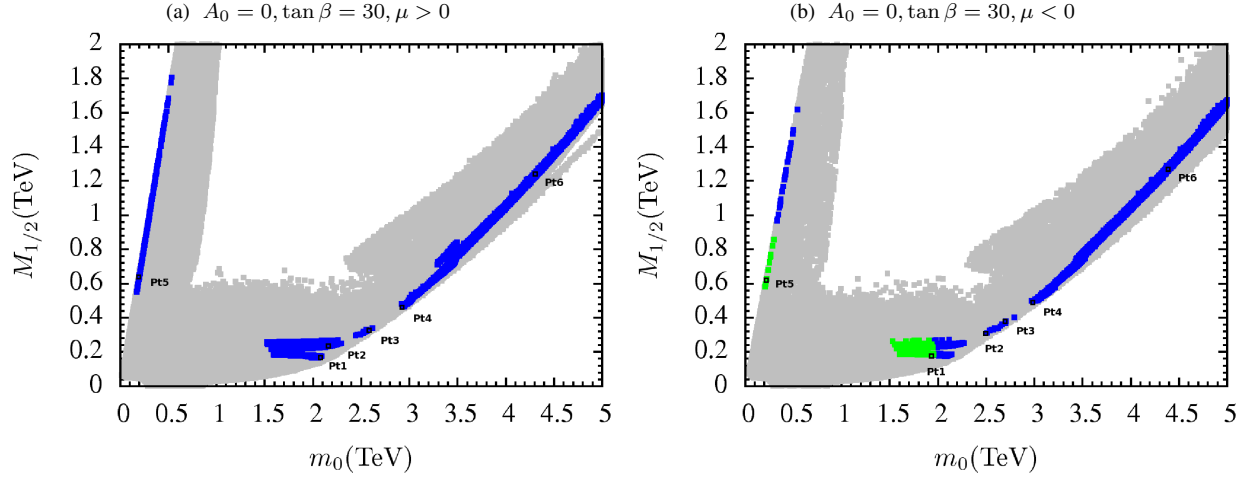


FIG. 4: Plots in the $(M_{1/2}, m_0)$ plane. Gray points are consistent with REWSB and $\tilde{\chi}_1^0$ LSP. Blue points satisfy the WMAP bounds on $\tilde{\chi}_1^0$ dark matter abundance, particle mass bounds, constraints from $BR(B_s \rightarrow \mu^+ \mu^-)$, $BR(b \rightarrow s \gamma)$ and $BR(B_u \rightarrow \tau \nu_\tau)$. Green points belong to the subset of blue points that satisfies all constraints including $\Delta(g-2)_\mu/2$. Approximate locations of benchmark points listed in Tables III and IV are also shown.

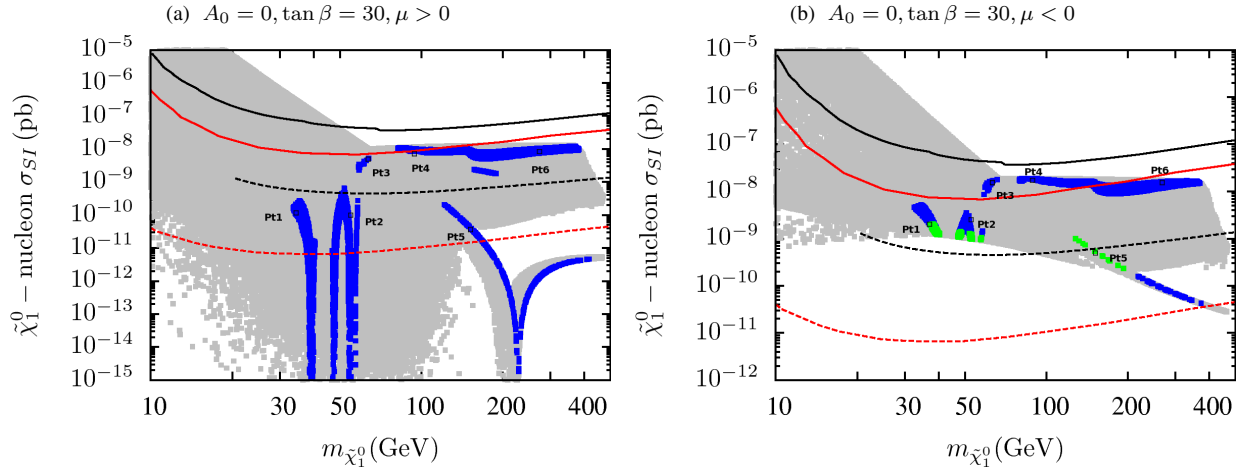


FIG. 5: Spin-independent elastic scattering cross section of neutralino dark matter in the $(\sigma_{SI}, m_{\tilde{\chi}_1^0})$ plane. Color coding is the same as in Figure 4. Current upper bounds from CDMS-II (XENON100) are depicted as solid black (red) lines. Future reach of SuperCDMS(SNOLAB) (dotted black line) and XENON1T (dotted red line) are shown. Approximate locations of benchmark points listed in Tables III and IV are also shown.

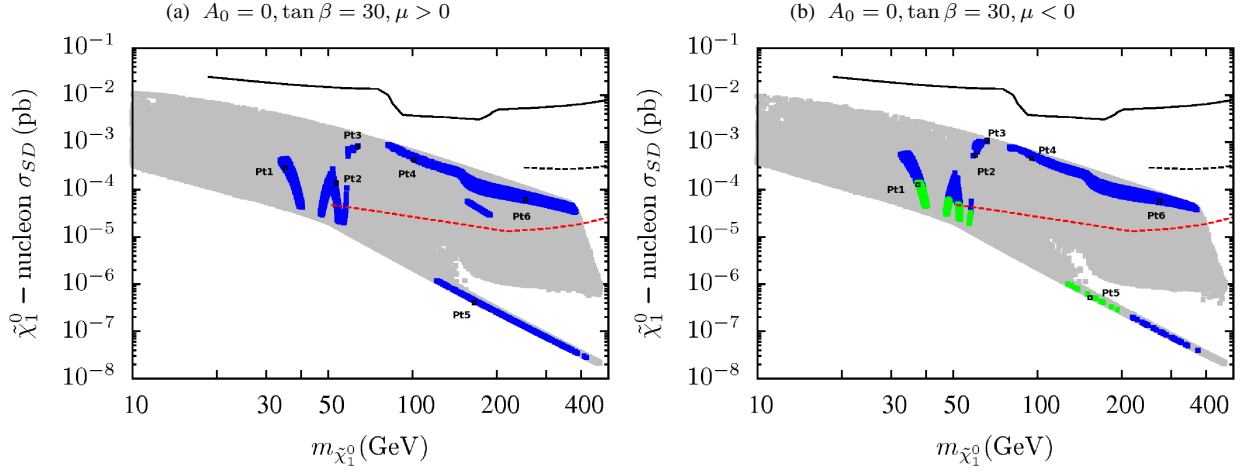


FIG. 6: Spin-dependent elastic scattering cross section of neutralino dark matter in the $(\sigma_{SD}, m_{\tilde{\chi}_1^0})$ plane. Color coding is the same as in Figure 4. Current upper bounds from Super-Kamiokande (black line), IceCube (dotted black line), and future reach of IceCube DeepCore (dotted red line) are shown. Approximate locations of benchmark points listed in Tables III and IV are also shown.

	Pt1	Pt2	Pt3	Pt4	Pt5	Pt6
m_0	2038	2158	2616	2980	201	4382
$M_{1/2}$	166	245	341	488	650	1280
A_0	0	0	0	0	0	0
$sign(\mu)$	+	+	+	+	+	+
$\tan \beta$	30	30	30	30	30	30
m_h	115	116	117	118	115	120
m_H	1734	1852	2247	2578	800	3939
m_A	1723	1840	2232	2561	795	3914
m_{H^\pm}	1737	1853	2248	2579	804	3940
$m_{\tilde{\chi}_{1,2}^0}$	34, 110	52, 169	64, 123	91, 137	144, 581	283, 337
$m_{\tilde{\chi}_{3,4}^0}$	138, 250	189, 345	124, 463	148, 651	596, 831	349, 1677
$m_{\tilde{\chi}_{1,2}^\pm}$	104, 245	160, 337	103, 450	119, 633	565, 818	311, 1641
$m_{\tilde{g}}$	503	696	934	1276	1486	2990
$m_{\tilde{u}_{L,R}}$	2049, 2052	2202, 2199	2694, 2685	3132, 3109	1444, 1301	5077, 4949
$m_{\tilde{t}_{1,2}}$	1184, 1604	1289, 1738	1595, 2137	1888, 2510	1068, 1355	3264, 4235
$m_{\tilde{d}_{L,R}}$	2051, 2053	2204, 2201	2695, 2686	3133, 3110	1446, 1300	5077, 4950
$m_{\tilde{b}_{1,2}}$	1593, 1903	1727, 2044	2125, 2499	2497, 2901	1258, 1341	4217, 4667
$m_{\tilde{\nu}_1}$	2040	2166	2632	3012	666	4544
$m_{\tilde{\nu}_3}$	1960	2082	2531	2898	650	4381
$m_{\tilde{e}_{L,R}}$	2041, 2036	2167, 2157	2632, 2614	3012, 2978	673, 233	4544, 4384
$m_{\tilde{\tau}_{1,2}}$	1874, 1960	1985, 2083	2408, 2531	2744, 2898	152, 659	4038, 4379
$\sigma_{SI}(\text{pb})$	1.6×10^{-10}	1.5×10^{-10}	5.2×10^{-9}	9.5×10^{-9}	6.0×10^{-11}	8.9×10^{-9}
$\sigma_{SD}(\text{pb})$	4.2×10^{-4}	1.0×10^{-4}	8.4×10^{-3}	6.5×10^{-4}	7.0×10^{-7}	5.9×10^{-5}
$\Omega_{CDM} h^2$	0.13	0.11	0.13	0.1	0.1	0.1

TABLE III: Mass spectra for the benchmark points for $\tan \beta=30$, $\mu > 0$. All of these points satisfy the various constraints mentioned in section III, except $\Delta(g-2)_\mu/2$. For all points, the neutralino LSP has sizeable higgsino component. The points lie between present and future direct and indirect dark matter search limits shown in Figures 5 and 6. Pt1 represents lightest neutralino scenario and Pt5 shows stau-coannihilation scenario.

	Pt1	Pt2	Pt3	Pt4	Pt5	Pt6
m_0	1939	2510	2790	3070	219	4490
$M_{1/2}$	183	311	402	525	616	1340
A_0	0	0	0	0	0	0
$sign(\mu)$	-	-	-	-	-	-
$\tan\beta$	30	30	30	30	30	30
m_h	115	117	118	119	115	121
m_H	1640	2139	2390	2650	695	400
m_A	1629	2125	2374	2630	690	3970
m_{H^\pm}	1642	2141	2391	2650	700	4000
$m_{\tilde{\chi}_{1,2}^0}$	37,142	59,130	66,112	96,142	136,553	290,337
$m_{\tilde{\chi}_{3,4}^0}$	177,279	135,425	126,541	157,700	569,791	355,1750
$m_{\tilde{\chi}_{1,2}^\pm}$	142,276	123,417	104,530	138,686	559,784	344,1720
$m_{\tilde{g}}$	542	861	1078	1360	1420	3100
$m_{\tilde{u}_{L,R}}$	1960,1961	2576,2568	2896,2881	3240,3200	1380,1240	5200,5090
$m_{\tilde{t}_{1,2}}$	1137,1534	1519,2035	1728,2303	1960,2600	1020,1280	3370,4350
$m_{\tilde{d}_{L,R}}$	1962,1963	2577,2570	2897,2884	3240,3220	1380,1240	5230,5090
$m_{\tilde{b}_{1,2}}$	1524,1810	2023,2382	2291,2679	2590,2990	1170,1270	4330,4780
$m_{\tilde{\nu}_1}$	1942	2523	2812	3110	641	4660
$m_{\tilde{\nu}_3}$	1865	2425	2704	2990	622	4490
$m_{\tilde{e}_{L,R}}$	1944,1938	2523,2508	2812,2788	3110,3070	648,247	4660,4490
$m_{\tilde{\tau}_{1,2}}$	1779,1866	2307,2425	2566,2703	2820,2990	145,633	4130,4490
$\sigma_{SI}(\text{pb})$	1.9×10^{-9}	8.6×10^{-9}	1.8×10^{-8}	1.7×10^{-8}	7.9×10^{-10}	1.5×10^{-8}
$\sigma_{SD}(\text{pb})$	1.4×10^{-4}	5.3×10^{-4}	1.0×10^{-3}	5.3×10^{-4}	8.4×10^{-7}	6.0×10^{-5}
$\Omega_{CDM}h^2$	0.13	0.12	0.13	0.1	0.13	0.1

TABLE IV: Mass spectra for the benchmark points for $\tan\beta=30$, $\mu < 0$. All of these points satisfy the various constraints mentioned in section III. For all points, the neutralino LSP has sizeable higgsino component. The points lie between present and future direct and indirect dark matter search limits shown in Figures 5 and 6. Pt1 shows the lightest neutralino and also a light gluino. Pt5 shows a stau-coannihilation scenario.

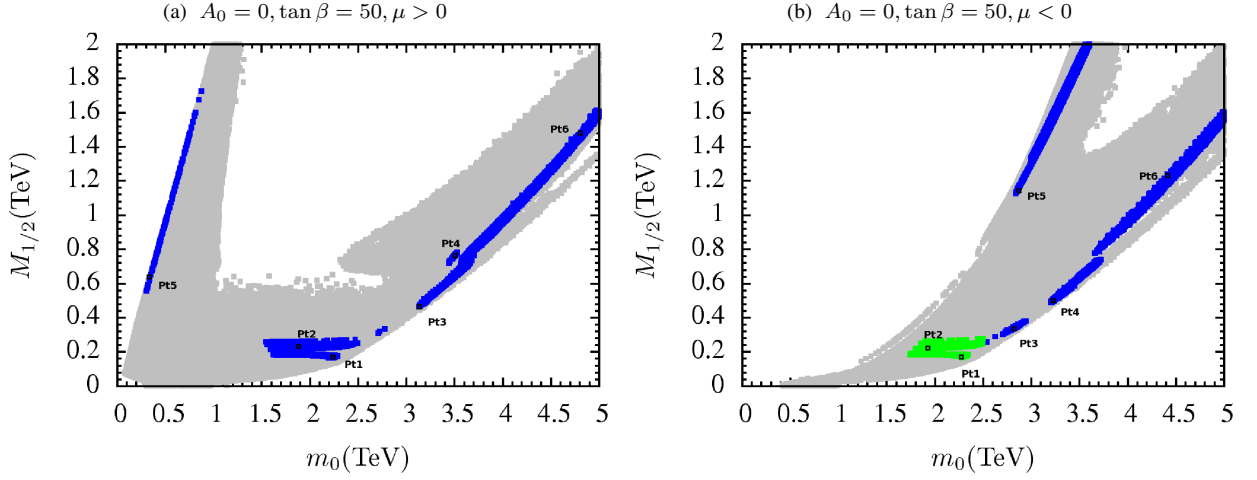


FIG. 7: Plots in the $(M_{1/2}, m_0)$ plane. Gray points are consistent with REWSB and $\tilde{\chi}_1^0$ LSP. Blue points satisfy the WMAP bounds on $\tilde{\chi}_1^0$ dark matter abundance, particle mass bounds, constraints from $BR(B_s \rightarrow \mu^+ \mu^-)$, $BR(b \rightarrow s \gamma)$ and $BR(B_u \rightarrow \tau \nu_\tau)$. Green points belong to the subset of blue points that satisfies all constraints including $\Delta(g-2)_\mu/2$. Approximate locations of benchmark points listed in Tables V and VI are also shown.

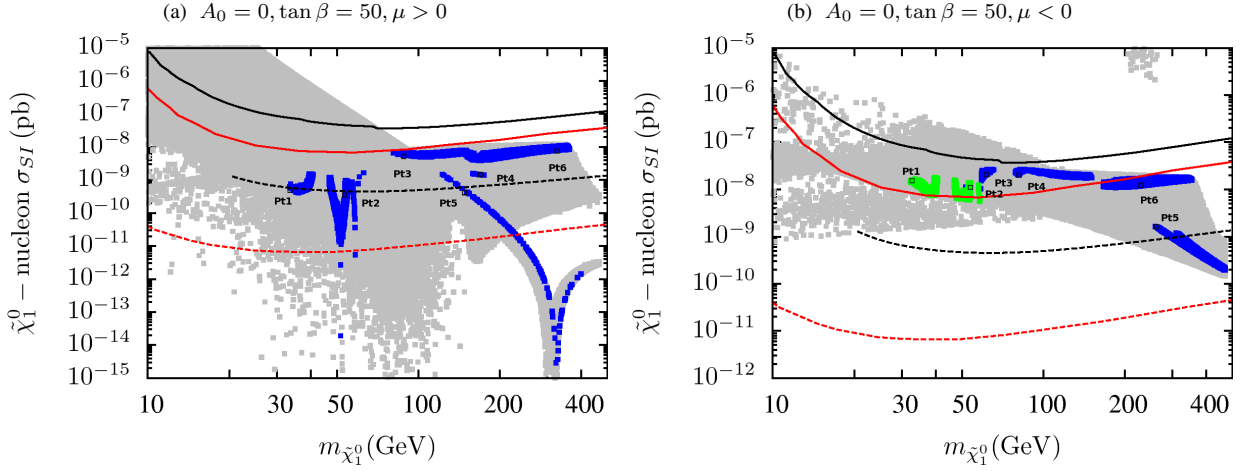


FIG. 8: Spin-independent elastic scattering cross section of neutralino dark matter in the $(\sigma_{SI}, m_{\tilde{\chi}_1^0})$ plane. Color coding is same as in Figure 4. Current upper bounds from the CDMS-II (XENON100) are depicted as solid black (red) lines. Future reach of SuperCDMS(SNOLAB) (dotted black line) and XENON1T (dotted red line) are shown. Approximate locations of benchmark points listed in Tables V and VI are also shown.

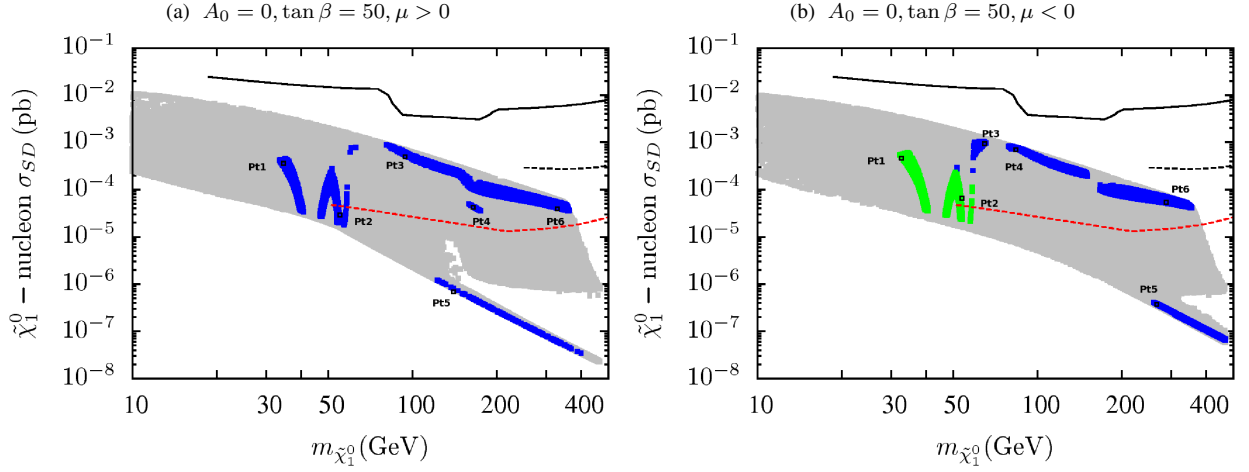


FIG. 9: Spin-dependent elastic scattering cross section versus neutralino dark matter mass. Color coding is the same as in Figure 4. Current bounds from Super-Kamiokande (black line) and IceCube (dotted black line), and future reach of IceCube DeepCore (dotted red line) are shown. Approximate locations of benchmark points listed in Tables V and VI are also shown.

	Pt1	Pt2	Pt3	Pt4	Pt5	Pt6
m_0	2241	1851	3175	3529	392	4765
$M_{1/2}$	167	247	489	783	735	1440
A_0	0	0	0	0	0	0
$sign(\mu)$	+	+	+	+	+	+
$\tan \beta$	50	50	50	50	50	50
m_h	116	115	119	120	116	121
m_H	1046	967	1609	1944	750	2802
m_A	1039	961	1598	1932	745	2785
m_{H^\pm}	1050	972	1613	1947	755	2803
$m_{\tilde{\chi}_{1,2}^0}$	33, 111	54, 225	90, 136	175, 287	165, 642	320, 371
$m_{\tilde{\chi}_{3,4}^0}$	138, 252	257, 357	148, 654	287, 1032	655, 938	386, 1886
$m_{\tilde{\chi}_{1,2}^\pm}$	104, 247	218, 350	119, 636	264, 1007	623, 923	344, 1845
$m_{\tilde{g}}$	509	693	1284	1928	1669	3326
$m_{\tilde{u}_{L,R}}$	2249, 2253	1913, 1906	3317, 3296	3868, 3808	1649, 1490	5564, 5416
$m_{\tilde{t}_{1,2}}$	1300, 1578	1130, 1387	1993, 2423	2407, 2934	1210, 1508	3593, 4386
$m_{\tilde{d}_{L,R}}$	2251, 2255	1914, 1907	3318, 3298	3868, 3809	1651, 1489	5565, 5417
$m_{\tilde{b}_{1,2}}$	1564, 1777	1373, 1545	2407, 2672	2917, 3170	1375, 1496	4362, 4614
$m_{\tilde{\nu}_1}$	2242	1862	3205	3604	817	4954
$m_{\tilde{\nu}_3}$	1984	1654	2850	3217	770	4444
$m_{\tilde{e}_{L,R}}$	2243, 2239	1864, 1850	3206, 3173	3604, 3528	823, 414	4953, 4768
$m_{\tilde{\tau}_{1,2}}$	1683, 1984	1397, 1654	2400, 2859	2677, 3215	173, 779	3621, 4440
$\sigma_{SI}(\text{pb})$	6.3×10^{-10}	4.5×10^{-10}	6.2×10^{-9}	1.4×10^{-9}	2.5×10^{-10}	8.9×10^{-9}
$\sigma_{SD}(\text{pb})$	4.2×10^{-4}	2.7×10^{-5}	6.5×10^{-4}	3.6×10^{-5}	4.9×10^{-7}	4.9×10^{-5}
$\Omega_{CDM} h^2$	0.13	0.11	0.1	0.13	0.13	0.1

TABLE V: Benchmark points for $\tan \beta=50$, $\mu > 0$. All of these points satisfy the various constraints mentioned in section III, except $\Delta(g-2)_\mu/2$. In all cases, the neutralino LSP has sizeable higgsino component. The points lie between present and future direct and indirect searches of dark matter shown in Figures 8 and 9. Pt1 represents lightest neutralino, and Pt5 shows stau-coannihilation scenario. Pts.1, and 2 show relatively light gluinos.

	Pt1	Pt2	Pt3	Pt4	Pt5	Pt6
m_0	2237	1944	2893	3248	2856	4495
$M_{1/2}$	174	246	368	509	1148	1259
A_0	0	0	0	0	0	0
$sign(\mu)$	-	-	-	-	-	-
$\tan\beta$	50	50	50	50	50	50
m_h	116	115	118	119	119	121
m_H	902	618	1276	1486	593	2200
m_A	896	614	1267	1476	589	2185
m_{H^\pm}	907	624	1279	1489	600	2202
$m_{\tilde{\chi}_{1,2}^0}$	34, 115	53, 217	64, 117	84, 121	265, 745	276, 330
$m_{\tilde{\chi}_{3,4}^0}$	143, 264	251, 358	124, 498	145, 679	749, 1487	344, 1650
$m_{\tilde{\chi}_{1,2}^\pm}$	114, 259	219, 355	108, 487	116, 666	760, 1465	336, 1625
$m_{\tilde{g}}$	527	693	1001	1330	2643	2949
$m_{\tilde{u}_{L,R}}$	2248, 2251	2001, 1995	2975, 2965	3399, 3376	3711, 3562	5154, 5033
$m_{\tilde{t}_{1,2}}$	1302, 1554	1181, 1381	1764, 2115	2047, 2457	2469, 2880	3300, 3957
$m_{\tilde{d}_{L,R}}$	2250, 2253	2003, 1996	2976, 2967	3398, 3378	3712, 3561	5154, 5034
$m_{\tilde{b}_{1,2}}$	1539, 1730	1366, 1495	2099, 2333	2440, 2686	2791, 2861	3935, 4137
$m_{\tilde{\nu}_1}$	2239	1955	2910	3281	3059	4648
$m_{\tilde{\nu}_3}$	1973	1717	2575	2906	2704	4135
$m_{\tilde{e}_{L,R}}$	2240, 2235	1956, 1942	2911, 2891	3281, 3246	3060, 2861	4648, 4496
$m_{\tilde{\tau}_{1,2}}$	1662, 1974	1424, 1718	2163, 2574	2432, 2906	2017, 2701	3341, 4131
$\sigma_{SI}(\text{pb})$	1.3×10^{-8}	1.0×10^{-8}	2.6×10^{-8}	2.6×10^{-8}	1.5×10^{-9}	1.4×10^{-8}
$\sigma_{SD}(\text{pb})$	3.7×10^{-4}	3.0×10^{-5}	7.8×10^{-4}	7.8×10^{-4}	3.8×10^{-7}	5.9×10^{-5}
$\Omega_{CDM} h^2$	0.13	0.11	0.12	0.11	0.11	0.12

TABLE VI: Benchmark points for $\tan\beta=50$, $\mu < 0$. All of these points satisfy the various constraints mentioned in section III. For all points, the neutralino LSP has sizeable higgsino component. The points lie between present and future direct and indirect dark matter search limits shown in Figures 8 and 9. Pt1 shows lightest neutralino and a light gluino. Pt5 shows stau-coannihilation.

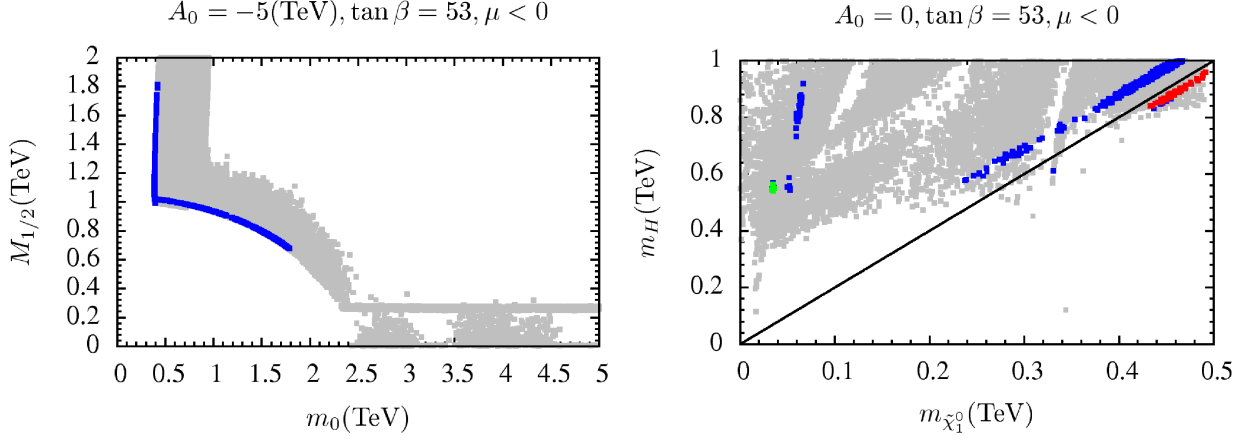


FIG. 10: Plots in the $(M_{1/2}, m_0)$ and $(m_H, m_{\tilde{\chi}_1^0})$ planes. Gray points are consistent with REWSB and $\tilde{\chi}_1^0$ LSP. Blue points satisfy the WMAP bounds on $\tilde{\chi}_1^0$ dark matter abundance, particle mass bounds, constraints from $BR(B_s \rightarrow \mu^+ \mu^-)$, $BR(b \rightarrow s\gamma)$ and $BR(B_u \rightarrow \tau \nu_\tau)$. Green points belong to the subset of blue points that satisfies all constraints including $\Delta(g-2)_\mu/2$. Red points satisfy criterion of $|2m_{\tilde{\chi}_1^0} - m_H| \leq 30$.

	Pt1	Pt2	Pt3
m_0	1771	1751	4892
$M_{1/2}$	686	696	2075
A_0	-5000	-5000	0
$sign(\mu)$	-	-	-
$\tan \beta$	10	10	53
m_h	123	122	122
m_H	2657	2650	947
m_A	2640	2633	940
m_{H^\pm}	2658	2652	951
$m_{\tilde{\chi}_{1,2}^0}$	154, 879	156, 892	488, 879
$m_{\tilde{\chi}_{3,4}^0}$	1929, 1932	1934, 1938	880, 2696
$m_{\tilde{\chi}_{1,2}^\pm}$	886, 1938	899, 1944	900, 2658
$m_{\tilde{g}}$	1648	1669	4578
$m_{\tilde{u}_{L,R}}$	2303, 2217	2303, 2214	6398, 6119
$m_{\tilde{t}_{1,2}}$	188, 1695	196, 1697	4289, 5030
$m_{\tilde{d}_{L,R}}$	2305, 2218	2304, 2215	6398, 6119
$m_{\tilde{b}_{1,2}}$	1700, 2144	1703, 2141	4876, 5001
$m_{\tilde{\nu}_1}$	1889	1873	5270
$m_{\tilde{\nu}_3}$	1865	1849	4597
$m_{\tilde{e}_{L,R}}$	1887, 1775	1872, 1755	5270, 4901
$m_{\tilde{\tau}_{1,2}}$	1717, 1864	1697, 1849	3270, 4592
$\sigma_{SI}(\text{pb})$	1.2×10^{-11}	1.2×10^{-11}	7.8×10^{-10}
$\sigma_{SD}(\text{pb})$	1.4×10^{-9}	2.3×10^{-9}	5.2×10^{-7}
$\Omega_{CDM} h^2$	0.12	0.13	0.1

TABLE VII: Pts.1 and 2 correspond to stop-neutralino coannihilation region, while Pt3 belongs in the so-called H-funnel region.

	NUGM	CMSSM	NUGM	CMSSM	NUGM	CMSSM	NUGM	CMSSM
m_0	287	199	538	268	219	150	440	276
$M_{1/2}$	1687	918	1188	650	1258	691	1040	572
A_0	1000	1000	1000	1000	1000	1000	1000	1000
$sign(\mu)$	-	-	-	-	+	+	+	+
$\tan \beta$	10	10	30	30	10	10	30	30
m_h	118	116	118	115	117	115	117	115
m_H	2071	1160	1289	726	1587	888	1233	687
m_A	2057	1152	1281	721	1576	882	1225	683
m_{H^\pm}	2073	1163	1292	731	1589	892	1236	692
$m_{\tilde{\chi}_{1,2}^0}$	388, 1277	388, 732	271, 933	271, 509	287, 1005	287, 538	236, 840	236, 442
$m_{\tilde{\chi}_{3,4}^0}$	1281, 2146	976, 984	940, 1512	704, 716	1011, 1597	750, 767	847, 1322	628, 644
$m_{\tilde{\chi}_{1,2}^\pm}$	1298, 2121	733, 983	948, 1496	509, 715	971, 1574	539, 767	811, 1302	443, 645
$m_{\tilde{g}}$	3594	2020	2601	1470	2736	1553	2298	1307
$m_{\tilde{u}_{L,R}}$	3474, 3084	1848, 1776	2557, 2293	1364, 1315	2645, 2357	1423, 1369	2252, 2021	1220, 1178
$m_{\tilde{t}_{1,2}}$	2547, 3285	1490, 1751	1875, 2363	1095, 1273	2502, 1235	1145, 1358	1655, 2102	975, 1148
$m_{\tilde{d}_{L,R}}$	3475, 3080	1850, 1769	2558, 2290	1366, 1310	2646, 2354	1425, 1364	2253, 2019	1223, 1174
$m_{\tilde{b}_{1,2}}$	3065, 3268	1727, 1760	2180, 2348	1230, 1270	2344, 2487	1330, 1359	1960, 2086	1108, 1151
$m_{\tilde{\nu}_1}$	1644	636	1269	505	1234	479	1101	466
$m_{\tilde{\nu}_3}$	1627	628	1211	478	1221	472	1056	433
$m_{\tilde{e}_{L,R}}$	1651, 398	645, 393	1275, 576	513, 362	1242, 301	489, 298	1107, 476	475, 350
$m_{\tilde{\tau}_{1,2}}$	388, 1640	388, 640	276, 1220	276, 496	290, 286	290, 484	241, 1064	241, 450
$\sigma_{SI}(\text{pb})$	5.4×10^{-11}	5.0×10^{-12}	9.9×10^{-11}	3.7×10^{-11}	7.5×10^{-13}	3.6×10^{-10}	3.0×10^{-10}	1.1×10^{-9}
$\sigma_{SD}(\text{pb})$	3.4×10^{-8}	1.0×10^{-7}	1.2×10^{-7}	4.2×10^{-7}	8.5×10^{-8}	3.1×10^{-7}	7.1×10^{-7}	7.0×10^{-7}
$\Omega_{CDM} h^2$	0.13	0.13	0.12	0.08	0.12	0.12	0.11	0.08

TABLE VIII: Particle masses for NUGM and CMSSM benchmark points in the stau-neutralino coannihilation region. The parameters m_0 and $M_{1/2}$ in the CMSSM are tuned so as to yield the same neutralino LSP and $\tilde{\tau}$ masses as in the NUGM for each benchmark point. We observe that masses of remaining particles can differ widely. Results for $\Omega_{CDM} h^2$ in CMSSM are within 5- σ range of the WMAP constraints.

	NUGM	CMSSM	NUGM	CMSSM	NUGM	CMSSM	NUGM	CMSSM
m_0	541	423	1690	1690	1700	1699	1684	1683
$M_{1/2}$	1203	1218	201	203	187	188	217	219
A_0	1000	1000	-1000	-1000	0	0	0	0
$sign(\mu)$	-	-	+	+	-	-	+	+
$\tan \beta$	30	30	30	30	30	30	50	50
m_h	118	119	115	115	114.4	115	114.4	114.5
m_H	1303	1318	1472	1461	1439	1444	875	781
m_A	1294	1310	1463	1451	1429	1434	869	775
m_{H^\pm}	1305	1321	1475	1463	1441	1446	880	786
$m_{\tilde{\chi}_{1,2}^0}$	275,940	523,980	44,248	85,165	39,172	77,141	47,208	89,162
$m_{\tilde{\chi}_{3,4}^0}$	947,1531	1243,1252	408,421	472,480	219,295	254,271	247,325	289,312
$m_{\tilde{\chi}_{1,2}^\pm}$	956,1514	981,1252	247,423	166,482	172,294	139,272	202,320	163,311
$m_{\tilde{g}}$	2631	2631	583	583	546	546	617	617
$m_{\tilde{u}_{L,R}}$	2582,2318	2423,2328	1731,1728	1725,1729	1732,1730	1726,1730	1736,1730	1727,1730
$m_{\tilde{t}_{1,2}}$	1896,2390	1939,2242	977,1349	964,1331	1010,1357	1012,1353	1023,1256	1025,1232
$m_{\tilde{d}_{L,R}}$	2587,2315	2423,2315	1733,1729	1726,1729	1734,1731	1727,1731	1737,1731	1730,1731
$m_{\tilde{b}_{1,2}}$	2205,2376	2202,2236	1337,1594	1318,1583	1346,1540	1341,1597	1241,1399	1215,1373
$m_{\tilde{\nu}_1}$	1283	905	1697	1691	1705	1699	1693	1685
$m_{\tilde{\nu}_3}$	1226	876	1625	1614	1636	1631	1502	1480
$m_{\tilde{e}_{L,R}}$	1289,580	912,616	1698,1690	1692,1690	1707,1699	1700,1699	1695,1683	1686,1683
$m_{\tilde{\tau}_{1,2}}$	278,1233	541,890	1542,1627	1532,1616	1558,1638	1562,1633	1269,1504	1240,1482

TABLE IX: Comparison of particle masses of NUGM and CMSSM benchmark points with m_0 and $M_{1/2}$ in CMSSM tuned to give the same $m_{\tilde{g}}$ and $m_{\tilde{d}_R}$ as in NUGM.